Novel B and N Sites of One-Dimensional Boron Nitride Fiber: Efficient Performance and Mechanism in the Formaldehyde Capture Process

Wenjing Yuan,* Yaoyao Wu, Tao Qi, Yinhua Wan, Shuping Zhang, Baozhi zhang, Hengcheng Zhou, Lili Shi, Guan Peng, and Shaoyuan Shi*

ACCESS | 📊 Metrics & More | 📖 Article Recommendations | 🆂🅸 Supporting Information

ABSTRACT: Identification of adsorption centers with atomic levels of adsorbents is crucial to study the adsorption of formaldehyde (HCHO), especially for an in-depth understanding of the mechanism of HCHO capture. Herein, we investigate the HCHO adsorption performance of one-dimensional (1D) nanoporous boron nitride (BN) fiber, and explore the adsorption mechanism by density functional theory (DFT) calculations, including adsorption energy change and Bader charge change, and experimental study as well. Research shows that the 1D nanoporous BN fiber possesses a high concentration of Lewis pairs, which act as Lewis acid and Lewis base sites associated with the fiber's electron-deficient and electron-rich features. It is worth noting that the HCHO removal efficiency of a typical sample is as high as 91%. This work may open the door to the field of adsorption of other pollutants by constructing Lewis pairs in the future.

● B   ● O   ● H   ● N   ● C
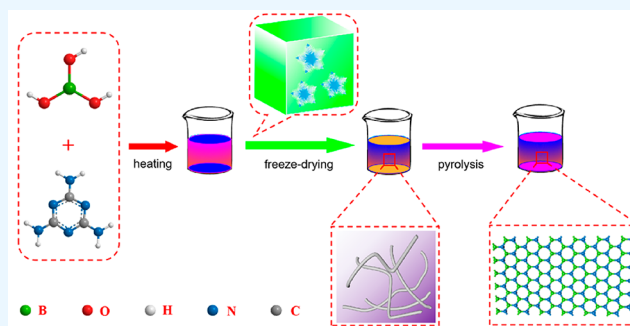
1. INTRODUCTION

Indoor air quality is closely related to human health, which is based on the fact that people usually spend most of their time in offices, houses, and other indoor places. HCHO, as one of the most dangerous volatile organic compounds, is released from building materials, wooden furniture, and so on.[1−5] Exposure to HCHO in the long term can cause a series of health problems, such as nausea, headache, allergic asthma, and even cancer.[6−9] Effective removal of the indoor HCHO pollutant is the key to solve the problem. In comparison with other approaches, catalytic oxidation, a simple and economical technology, has been regarded as an efficient route for conversion of HCHO into CO_2 and H_2O to improve the indoor air quality.[10,11] However, as adsorption is the first step of catalytic oxidation, the HCHO adsorption ability of the surface of the catalyst often limits its catalytic oxidation efficiency, which requires a high HCHO adsorption capacity for the catalyst substrate.

Theoretically, the HCHO molecule contains two C−H bonds and one C═O bond, in which the carbon atom forms three σ bonds in three sp² hybrid orbitals, and one σ bond is formed with the oxygen atom. One p orbital of the carbon atom and one p orbital of the oxygen atom overlap with each other to form a π bond. The HCHO molecule contains a carbonyl group oxygen atom, which easily interacts with the Lewis acid, while the carbonyl group carbon atom tends to react with the Lewis base.[12,13] Therefore, the HCHO pollutant

can be adsorbed easily by the acid−base sites of the adsorbent surface based on the Lewis theory of acid−base reaction.

Hexagonal boron nitride (h-BN), as a "white graphene", has attracted increasing attention recently.[14−18] Due to the high electronegativity of the nitrogen atom, the electron pair in the sp² B−N bond is closer to the nitrogen atom, and hence, to the electron-rich nitrogen atom of the boron nitride layer, which acts as the Lewis base. Meanwhile, the electron-deficient boron atom of the boron nitride substrate shows the feature of a Lewis acid,[19−21] which can provide opportunities for practical applications, especially for the HCHO adsorption process originating from the combination between the HCHO molecule and the adsorption sites (B-site and N-site) on the surface of the substrate.

For an ideal adsorbent, a large surface area is also essential, because it can provide as many adsorption sites as possible. Therefore, the purpose of this work is to construct the one-dimensional (1D) nanoporous structure of BN with a high surface area by the freeze-drying and calcination process, and

evaluate the performance of HCHO adsorption on the surface of as-prepared products at room temperature. The investigations show that a typical sample shows a strong ability of adsorption toward the HCHO pollutant when it is exposed to a low-concentration-HCHO environment, which can be ascribed to the structural characteristics of high BET surface area ($462 \text{ m}^2 \text{ g}^{-1}$) and Lewis acid−base sites. In addition, the HCHO adsorption mechanism over the surface of the 1D nanoporous BN fiber is also studied through DFT calculations, and a deep understanding about the role of the boron and nitrogen sites of BN in the HCHO capture process is obtained.

2. EXPERIMENTAL SECTION

2.1. Chemicals. Boric acid (H_3BO_3, 99%) and melamine ($C_3H_6N_6$, 99%) were purchased from Shanghai Aladdin Biochemical Technology Co., Ltd. Nitrogen (N_2, 99.999%) was purchased from Foshan Deli Messel Gas Co., Ltd.

2.2. Synthesis of the 1D Nanoporous BN Fiber. Firstly, 3.15 g of $C_3N_6H_6$ and 4.64 g of H_3BO_3 were added into 100 mL of deionized water to obtain a mixed solution and heated at 90 °C under magnetic stirring for 4 h. Subsequently, the hot solution was quickly transferred to the refrigerator and freeze-dried for 3 days to form the dry 1D nanoporous BN fiber precursor. The growth mechanism of the precursor was associated with the reaction as follows[22]

$$2H_3BO_3 + C_3N_6H_6 \rightarrow C_3N_6H_6 \cdot 2H_3BO_3 \quad (1)$$
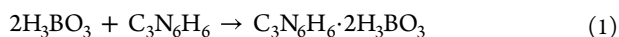
The $C_3N_6H_6 \cdot 2H_3BO_3$ nuclei were formed in hot solution by a hydrogen-bonded structure, which can absorb new nuclei continuously for construction of the 1D $C_3N_6H_6 \cdot 2H_3BO_3$ fiber. Then, the precursor was frozen quickly to prevent its further growth. Finally, the white $C_3N_6H_6 \cdot 2H_3BO_3$ precursor with a 1D fiber morphological structure was transformed into a 1D nanoporous BN fiber under the pyrolysis process in N_2 atmosphere at 800, 900, and 1000 °C for 4 h, and denoted as BN-800, BN-900, and BN-1000, respectively.

2.3. Characterization. The X-ray diffraction (XRD) patterns of the as-prepared samples were studied using an X-ray diffractometer (D-MAX 2200 VPC, RIGAKU). The morphology of a typical sample was studied using a scanning electron microscope (ZEISS, sigma 300) and a JEOL JEM-2100F transmission electron microscope. The surface element composition of the sample was obtained using an X-ray photoelectron spectrometer (Thermo ESCALAB 250XI). The Brunauer−Emmett−Teller (BET) surface area and pore size distribution of a typical sample were evaluated by a Tristar II 3020 instrument. The acid−base properties of the sample surface and the intermediates in the catalytic HCHO oxidation process were recorded using a TPD/TPR instrument (Quantachrome) and *in situ* diffuse reflection infrared Fourier transform spectroscopy (DRIFTS, Nicolet iS50).

2.4. HCHO Adsorption Measurement. The HCHO adsorption test was carried out using an organic glass box with a volume of 6.0 L at room temperature, and its inner wall was covered with an aluminum foil. Hundred milligrams of the 1D nanoporous BN fiber was uniformly dispersed on the bottom of a Petri dish with a diameter of 9 cm and covered with a lid. Gaseous HCHO was generated by injecting an appropriate amount of HCHO solution (37.0−40.0%). The lid was removed when the HCHO concentration in the organic glass box was stable at about 10 ppm. At this moment, the HCHO adsorption test began, and the real-time concentrations of

HCHO, CO_2, CO, and water vapor in the reactor were detected by a photoacoustic gas monitor (INNOVA 1412i).

2.5. Stability Test. The cyclic stability test over the typical sample was performed using the photoacoustic gas monitor (INNOVA 1412i). Briefly, 100 mg of 1D nanoporous BN fibers was dispersed on the bottom of the Petri dish with diameter 9 cm. When the initial HCHO concentration in the reactor reached about 10 ppm, the lid of the Petri dish was quickly removed to monitor the concentrations of HCHO, CO_2, CO, and water vapor in the reactor. The reaction ended after 120 min. Subsequently, the 1D nanoporous BN fibers were collected and transferred to an oven at 55 °C for 2 h. Finally, the collected sample was tested in the next cycle.

2.6. HCHO Adsorption Kinetics. The HCHO adsorption kinetics on the surface of the 1D nanoporous BN fiber was studied to investigate the adsorption behavior, which is achieved by fitting the kinetics models of pseudo-first-order and pseudo-second-order as below[23]

$$\ln(q_e - q_t) = \ln q_e - k_1 t \quad (2)$$

$$\frac{t}{q_t} = \frac{1}{k_2 q_e^2} + \frac{t}{q_e} \quad (3)$$

where k_1 (1/min), k_2 (g/mg/min), q_e, and q_t (mg/g) represent the rate constants of the pseudo-first-order and pseudo-second-order models, and the adsorption capacities at equilibrium and time t are shown in the following formulas[24]

$$q_e = \frac{(C_0 - C_e)V}{W} \quad (4)$$

$$q_t = \frac{(C_0 - C_t)V}{W} \quad (5)$$

where V (L) stands for the volume of the reactor and W (g) is the mass of the adsorbent. C_e, C_0, and C_t (mg L^{-1}) are the HCHO concentrations at equilibrium, initial time, and time t, respectively.

2.7. Calculation Details. DFT calculations were carried out with the Vienna Ab Initio Simulation Package (VASP) by using a spin-polarized GGA PBE functional combined with a projector augmented wave (PAW) method and an energy cutoff of 520 eV for all-electron plane-wave basis sets. The conjugate gradient algorithm was used in the optimization. A total energy of 1×10^{-4} eV and force of 0.05 eV Å^{-1} were set on each atom to the convergence threshold. The adsorption energy change (ΔE_{ads}) was calculated based on the following formula

$$\Delta E_{ads} = E_{total} - E_{sur} - E_{mol} \quad (6)$$

where E_{mol}, E_{sur}, and E_{total} denote the energy of the molecule, the energy of the pure surface, and the total energy of the adsorption state, respectively.

3. RESULTS AND DISCUSSION

Scanning electron microscopy observation shows that BN-900 is mainly composed of 1D fiber morphology, as presented in Figure 1a. This unique morphological structure of BN-900 may be ascribed to the $C_3N_6H_6 \cdot 2H_3BO_3$ precursor with 1D fiber morphology. Meanwhile, the 1D morphology of BN-900 is further confirmed by the transmission electron microscope image. In Figure 1b,c, the 1D fiber morphology of BN-900 can be clearly seen, and the surface structure is further analyzed
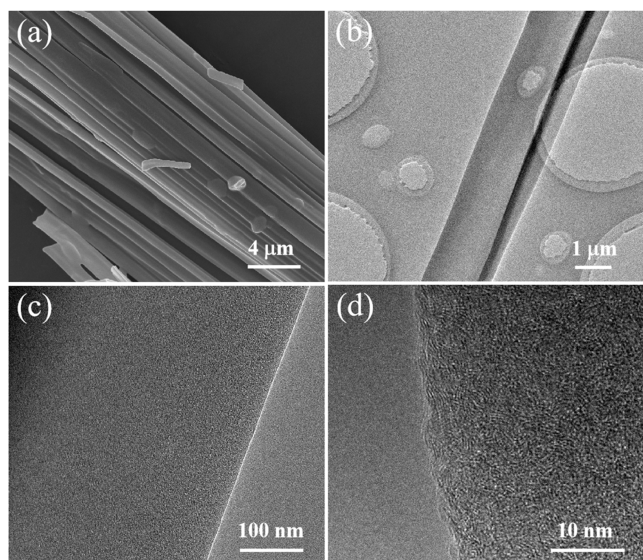
Figure 1. (a) SEM, (b-c) TEM, and (d) HRTEM images of BN-900.

using the high-resolution TEM. The 1D nanoporous BN fiber accompanied by an unordered and amorphous structure is observed as displayed in Figure 1d, suggesting that some defects are distributed on the surface of the 1D nanoporous BN fiber, and therefore the surface atom coordination is highly unsaturated, which is beneficial for adsorption of polar molecules, such as the HCHO pollutant.

In the XRD patterns of the as-prepared samples (Figure 2a), the (002) and (100) planes of BN are obtained, while the diffraction peaks at about 24 and 43° demonstrate an obviously broad peak feature, implying a low-crystallinity BN phase with disordered characteristics.[24,25] The XPS survey spectrum of

BN-900 is exhibited in Figure S1 (see the Supporting Information), and the signals of boron, nitrogen, carbon, and oxygen elements can be found clearly from the XPS survey spectrum of BN-900. Both B 1s and N 1s correspond to the BN phase, and the peak of C 1s is likely attributed to the adventitious hydrocarbon.[24] As shown in Figure 2b, the high-resolution B 1s XPS spectrum of BN-900 presents a main peak at about 190.9 eV associated with the B−N bond, and a minor peak at about 192.3 eV derived from the B−O bond, and the existence of the B−O bond may be due to the surface hydroxyl.[18] In addition, the N−B bond located at about 398.2 eV and the N−H bond centered at about 399.0 eV are clearly detected in the high-resolution N 1s XPS spectrum of the typical sample (Figure 2c), which is basically consistent with the reported data.[24] The porosity of the typical sample is evaluated by the nitrogen adsorption−desorption isotherms (Figure 2d). The characteristic of the curve belongs to the type IV isotherm, revealing the existence of a mesoporous structure in BN-900, which is also confirmed by the pore size distribution, as displayed in the inset of Figure 2d. The mesoporous structure in the range of about 3.0−4.4 nm in size is shown. Besides, the BET surface area of BN-900 is up to 462 m^2 g^{-1}, which can be attributed to the abundant porosity derived from the release of gaseous groups, such as NH_3, H_2O, and CO from the $C_3N_6H_6 \cdot 2H_3BO_3$ precursor.[22] Therefore, the typical sample can provide abundant adsorption sites to enhance the HCHO adsorption capacity on the surface of the 1D nanoporous BN fiber.

Encouraged by the above results, we deduce that the 1D nanoporous BN fiber may be a promising adsorbent to eliminate the indoor HCHO pollutant, and therefore the HCHO adsorption ability of the 1D nanoporous BN fiber is investigated. The HCHO adsorption performance comparison in Figure 3a shows the excellent adsorption ability of BN-900
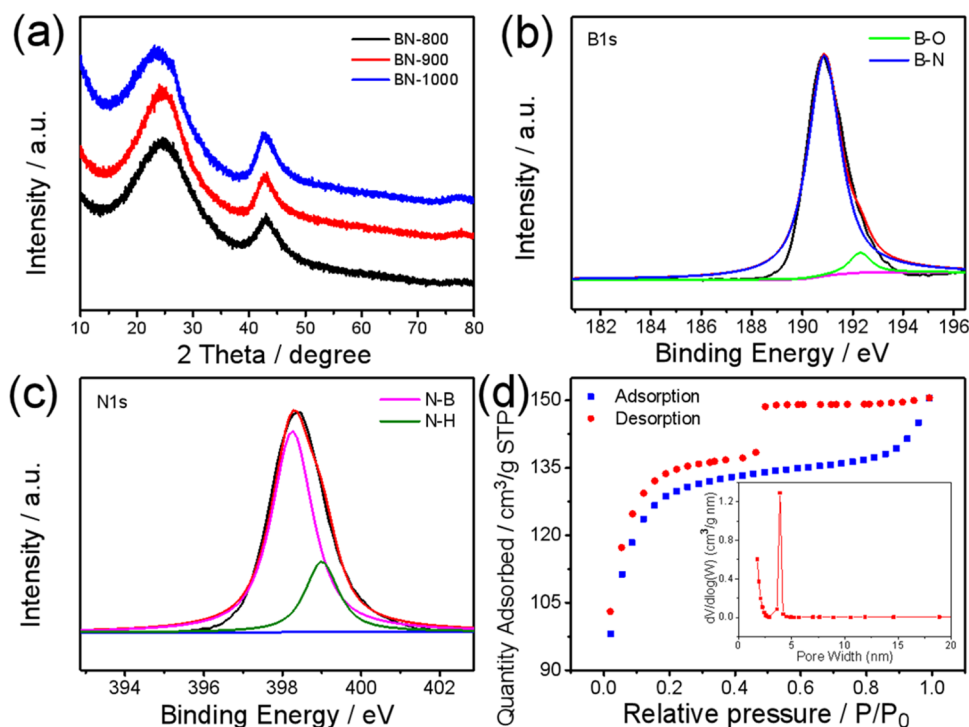

Figure 2. (a) XRD patterns of BN-800, BN-900, and BN-1000; high-resolution (b) B 1s and (c) N 1s XPS spectra, and (d) nitrogen adsorption−desorption isotherms and pore size distribution (inset) of BN-900.
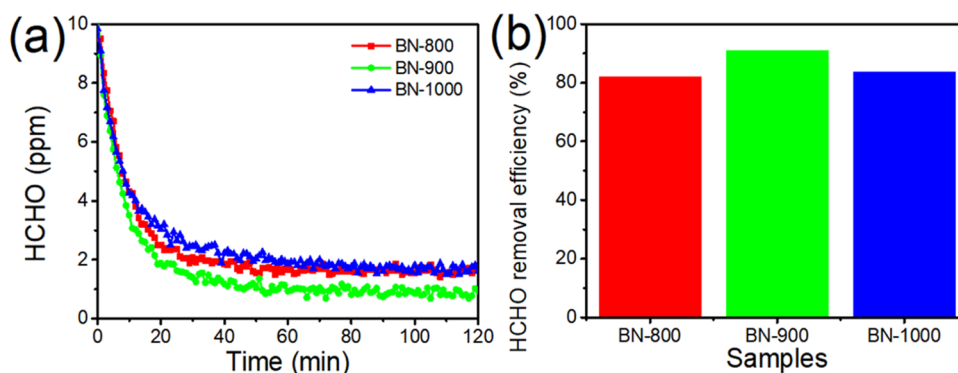
Figure 3. (a) Concentration changes of HCHO and (b) corresponding HCHO removal efficiency of the as-prepared samples.
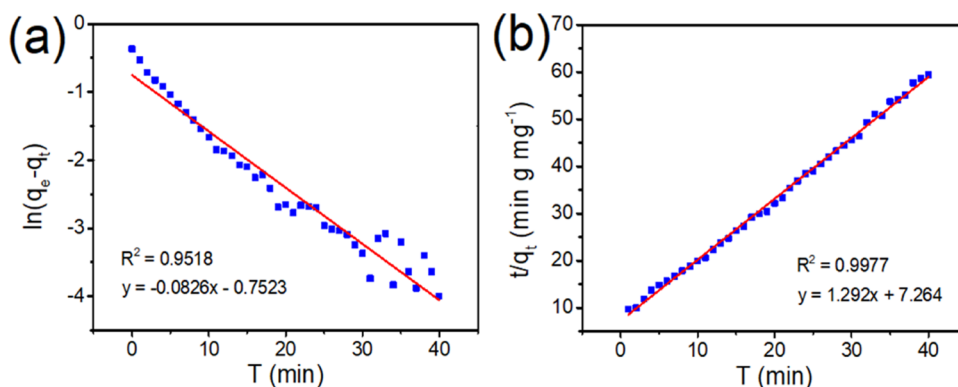

Figure 4. Data fitting of the HCHO adsorption kinetics of BN-900 by (a) pseudo-first-order and (b) pseudo-second-order models.

compared to that of BN-800 and BN-1000. The HCHO removal efficiency of the typical sample is as high as 91% at 120 min, as shown in Figure 3b. Though BN-800 and BN-1000 display relatively weak removal efficiencies, the values still reach 82 and 84%, respectively. In addition, the estimated adsorption capacity within 120 min is up to 0.59 mg g^{-1} (BN-800), 0.69 mg g^{-1} (BN-900), and 0.61 mg g^{-1} (BN-1000) based on Figure S2a (see the Supporting Information), implying that 1D nanoporous BN fibers have a significant potential application in improving indoor air quality. It is noteworthy that the concentrations of CO_2 in the HCHO adsorption process for 1D nanoporous BN fibers show no significant change (Figure S2b, see the Supporting Information), revealing that the 1D nanoporous BN fiber shows mainly adsorption rather than catalytic oxidation. As shown in Figure S2c,d (see the Supporting Information), the concentrations of CO and water vapor in the reaction system exhibit a slight downward trend, indicating that 1D nanoporous BN fibers have also a certain adsorption effect on the CO and H_2O. In addition, the stability evaluation of the adsorbent is crucial to ensure its practical application, and hence, the stability test of HCHO adsorption on BN-900 is conducted as shown in Figure S3a (see the Supporting Information). As can be seen in Figure S3b (see the Supporting Information), the HCHO removal efficiencies of the three cyclic tests over BN-900 are 91, 67, and 63%, respectively. It is worth noting that the HCHO removal efficiency shows a certain attenuation, which may be attributed to the strong adsorption configuration between the HCHO molecules and active sites of the BN-900 surface, and make it difficult to desorb and release active sites, further leading to the attenuation of HCHO adsorption performance. However, it reaches 63% in the third cycle,

suggesting that the 1D nanoporous BN fiber is still a promising adsorbent for purifying indoor HCHO.

In order to understand the adsorption behavior on the surface of the 1D nanoporous BN fiber, the HCHO adsorption process over BN-900 is fitted using the pseudo-first-order and pseudo-second-order models. Compared with the pseudo-first-order model (R^2 = 0.9518, Figure 4a), the fitting effect of the pseudo-second-order model (R^2 = 0.9977, Figure 4b) is better, indicating that the HCHO adsorption on the surface of the 1D nanoporous BN fiber shows chemisorption behavior, further confirming that the HCHO adsorption on the surface of the 1D nanoporous BN fiber is likely to be due to chemisorption, which results in the formation of adsorbed HCHO. The chemisorption behavior of the 1D nanoporous BN fiber is a promising structural feature, suggesting that the 1D nanoporous BN fiber has great potential in the purification of indoor HCHO pollution in the future. To explore the mechanism of chemisorption of HCHO on the adsorbent, the 1D nanoporous BN fibers with acid−base properties are analyzed by TPD of NH_3 and CO_2. The NH_3-TPD curve of BN-900 is exhibited in Figure S4 (see the Supporting Information); the peaks ranging from approximately 118 to 253 and 325 to 500 °C can be assigned to the weak acid and medium acid sites on the surface of the 1D nanoporous BN fiber. In the CO_2-TPD curve, the peak from approximately 115 to 269 °C is attributed to the weak base sites, and the range of 326 to 511 °C corresponds to the medium base sites. These unique acid−base features may be derived from the effect of electron-deficient B atoms and electron-rich N atoms on the surface of the 1D nanoporous BN fiber. It is worth noting that the Lewis pair is obtained, which means that the 1D nanoporous BN fiber can effectively capture the HCHO
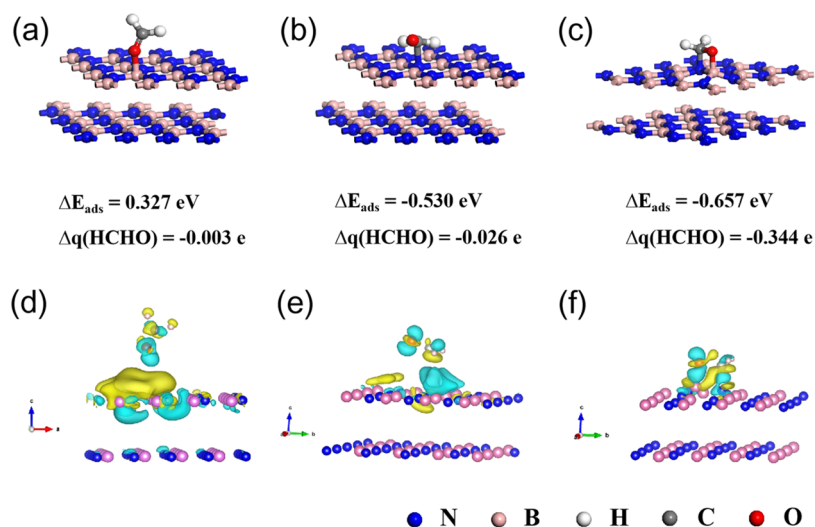
$\Delta E_{ads} = 0.327$ eV

$\Delta q(HCHO) = -0.003$ e

$\Delta E_{ads} = -0.530$ eV

$\Delta q(HCHO) = -0.026$ e

$\Delta E_{ads} = -0.657$ eV

$\Delta q(HCHO) = -0.344$ e

● N   ● B   ○ H   ● C   ● O

Figure 5. Structural models and charge density differences of HCHO adsorption on the surface of the 1D nanoporous BN fiber. (a, d) Oxygen, (b, e) carbon, and (c, f) oxygen and carbon atoms of HCHO are combined on boron, nitrogen, and boron and nitrogen atoms of BN models, respectively. The electron depletion is shown in yellow and accumulation in blue.

molecule *via* chemisorption based on the Lewis theory of acid−base reaction.

The Lewis acid and base sites on the surface of the 1D nanoporous BN fiber are confirmed by the TPD curves of NH_3 and CO_2. The DFT calculations also confirm that the HCHO adsorption on the surface of the 1D nanoporous BN fiber is focused on the combination of carbon and oxygen atoms of the HCHO molecule and the B−N Lewis pair structure, and therefore, the key parameters show that the combination state is the focal point of DFT analysis. The structural models of HCHO adsorption on the boron site (Figure 5a), nitrogen site (Figure 5b), and boron and nitrogen sites (Figure 5c) of BN are constructed. In comparison with the adsorption energy change (ΔE_{ads}) of B−O (0.327 eV) and N−C adsorption configuration (−0.530 eV), the double-site adsorption configuration of B−O and N−C (−0.657 eV) shows the most negative adsorption energy change, indicating a spontaneous adsorption reaction. To investigate the electron transfer in the process of HCHO adsorption on BN models, the charge density differences are calculated using the Vienna Ab Initio Simulation Package; the electron depletion is shown in yellow and accumulation in blue. As shown in Figure 5f, the charge density differences of B−O and N−C bonds between the HCHO molecule and BN model present a stronger interaction than that of the other two single-point adsorption models in terms of B−O (Figure 5d) and N−C (Figure 5e) adsorption configuration. In addition, the Bader charge change is chosen as a parameter to investigate the ability of the electrons to transfer onto the above structural models, and the corresponding values are −0.003e, −0.026e, and −0.344e. The most negative value of Bader charge change (Δq) of the double-site adsorption configuration of B−O and N−C bonds between the HCHO molecule and BN model indicates that the B−N Lewis pair structure of BN can adsorb the HCHO molecule effectively, revealing that the 1D nanoporous BN fiber is a promising candidate to capture the HCHO pollutant.

The intermediate species of the HCHO adsorption process over the typical sample is detected by *in situ* diffuse reflectance infrared Fourier transform spectroscopy under exposure to $HCHO/O_2$ at room temperature. As displayed in Figure 6, the peaks appearing at approximately 1413, 1700, and 1771 cm^{-1}
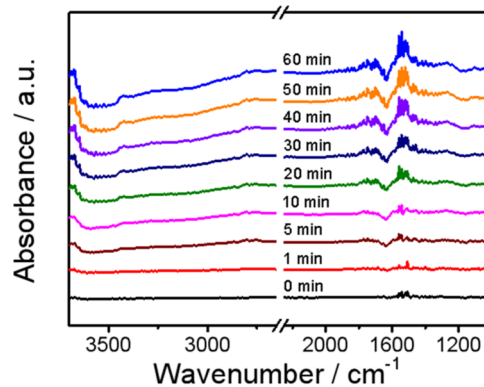

Figure 6. *In situ* DRIFTS of BN-900 under a flow of $HCHO/O_2$ at room temperature.

are associated with the adsorbed HCHO, and those at approximately 1340, 1362, 1372, 1395, 1455, 1540, 1558, 1649, 1700, 1825, and 1868 cm^{-1} involve the formate species.[26−28] Besides, the peak at approximately 1467 cm^{-1} is related to the methoxy group, and those from approximately 3200 to 3600 cm^{-1} result from the stretching vibration of the hydroxyl group.[24,29,30] Remarkably, the adsorbed water, located at about 1640 cm^{-1}, exhibits a strong negative peak, implying that the adsorbed water is consumed in the HCHO adsorption process on the surface of BN-900. The results show that the 1D nanoporous BN fiber with Lewis pair structure is able to catalyze the HCHO pollutant and convert it into low-toxic or nontoxic intermediate species. However, the peak of CO_2 is not observed obviously, and meanwhile, the intensities of the observed peaks of the intermediate species are also relatively weak, revealing that the contribution to HCHO removal efficiency is mainly by adsorption rather than by catalytic oxidation.

A possible adsorption and conversion HCHO mechanism is proposed herein, which may be related to the Cannizzaro-like disproportionation reaction under the current reaction system due to the feature of Lewis acid−base sites on the surface of the 1D nanoporous BN fiber. Firstly, the lone electron pair of N sites in the 1D nanoporous BN fiber triggers easily a

nucleophilic addition reaction when the HCHO molecule is adsorbed on the Lewis base N-site. Secondly, the HCHO attached to the Lewis acid B-site can enhance the electrophilicity ability of the carbon atom, and it can acquire one H atom of HCHO molecule derived from the N-site. As a result, formate and methoxy species are produced. Finally, the intermediate species is further converted into low-toxic or nontoxic species by the reaction with surface-adsorbed H_2O molecules, which is also confirmed based on the *in situ* DRIFTS, indicating that the 1D nanoporous BN fiber is a potential candidate for indoor HCHO purification in the future.

4. CONCLUSIONS

In summary, the B−N Lewis pair on the surface of the 1D nanoporous BN fiber has been successfully constructed and explored to capture the HCHO pollutant at room temperature. As proved by both theoretical and experimental results, the typical sample with abundant Lewis acid−base sites presents excellent HCHO adsorption and activation activity. The 1D nanoporous morphology structure of the as-prepared BN sample is significant, which results in a high BET surface area and is made up of B−N bonds, and can be used to further construct the Lewis pair for chemisorption of HCHO. This study provides a new understanding of HCHO adsorption on the B−N structure and points out the direction for application of the 1D nanoporous BN fiber.

■ ASSOCIATED CONTENT

Ⓢ Supporting Information

The Supporting Information is available free of charge at https://pubs.acs.org/doi/10.1021/acsomega.2c02920.

> Additional characterization (XPS and TPD), adsorption capacity, CO_2 concentration, CO concentration, water vapour, stability, and HCHO removal efficiency (PDF)

■ AUTHOR INFORMATION

Corresponding Authors

Wenjing Yuan − *Ganjiang Innovation Academy, Chinese Academy of Sciences, Ganzhou 341119, People's Republic of China; Jiangxi Province Key Laboratory of Cleaner Production of Rare Earths, Ganzhou 341119, People's Republic of China;* ⓞ orcid.org/0000-0001-6694-2867; Email: wjyuan@gia.cas.cn

Shaoyuan Shi − *Ganjiang Innovation Academy, Chinese Academy of Sciences, Ganzhou 341119, People's Republic of China; Jiangxi Province Key Laboratory of Cleaner Production of Rare Earths, Ganzhou 341119, People's Republic of China; Institute of Process Engineering, Chinese Academy of Sciences, Beijing 100190, People's Republic of China;* ⓞ orcid.org/0000-0002-0205-231X; Email: syshi@ipe.ac.cn

Authors

Yaoyao Wu − *School of Environmental Science and Engineering, Sun Yat-sen University, Guangzhou 510006, People's Republic of China*

Tao Qi − *Ganjiang Innovation Academy, Chinese Academy of Sciences, Ganzhou 341119, People's Republic of China; Jiangxi Province Key Laboratory of Cleaner Production of Rare Earths, Ganzhou 341119, People's Republic of China;*

Institute of Process Engineering, Chinese Academy of Sciences, Beijing 100190, People's Republic of China

Yinhua Wan − *Ganjiang Innovation Academy, Chinese Academy of Sciences, Ganzhou 341119, People's Republic of China; Jiangxi Province Key Laboratory of Cleaner Production of Rare Earths, Ganzhou 341119, People's Republic of China; Institute of Process Engineering, Chinese Academy of Sciences, Beijing 100190, People's Republic of China*

Shuping Zhang − *School of Chemical Engineering and Materials, Changzhou Institute of Technology, Changzhou 213032, People's Republic of China*

Baozhi zhang − *Ganjiang Innovation Academy, Chinese Academy of Sciences, Ganzhou 341119, People's Republic of China; Jiangxi Province Key Laboratory of Cleaner Production of Rare Earths, Ganzhou 341119, People's Republic of China*

Hengcheng Zhou − *Ganjiang Innovation Academy, Chinese Academy of Sciences, Ganzhou 341119, People's Republic of China; Jiangxi Province Key Laboratory of Cleaner Production of Rare Earths, Ganzhou 341119, People's Republic of China*

Lili Shi − *Ganjiang Innovation Academy, Chinese Academy of Sciences, Ganzhou 341119, People's Republic of China; Jiangxi Province Key Laboratory of Cleaner Production of Rare Earths, Ganzhou 341119, People's Republic of China*

Guan Peng − *Ganjiang Innovation Academy, Chinese Academy of Sciences, Ganzhou 341119, People's Republic of China; Jiangxi Province Key Laboratory of Cleaner Production of Rare Earths, Ganzhou 341119, People's Republic of China*

Complete contact information is available at:
https://pubs.acs.org/10.1021/acsomega.2c02920

Notes

The authors declare no competing financial interest.

■ ACKNOWLEDGMENTS

■ REFERENCES

(1) Peng, S.; Yang, X.; Strong, J.; Sarkar, B.; Jiang, Q.; Peng, F.; Liu, D.; Wang, H. MnO_2-Decorated N-Doped Carbon Nanotube with Boosted Activity for Low-Temperature Oxidation of Formaldehyde. *J. Hazard. Mater.* **2020**, *396*, No. 122750.

(2) Liu, F.; Liu, X.; Shen, J.; Bahi, A.; Zhang, S.; Wan, L.; Ko, F. The Role of Oxygen Vacancies on $Pt/NaInO_2$ Catalyst in Improving Formaldehyde Oxidation at Ambient Condition. *Chem. Eng. J.* **2020**, *395*, No. 125131.

(3) Xie, H.; Chen, X.; Zhang, C.; Lao, Z.; Liu, X.; Xie, X.; Semiat, R.; Zhong, Z. Identifying the $Fe_3Mn_3O_8$ Phase as a Superior Catalyst for Low-Temperature Catalytic Oxidation of Formaldehyde in air. *Environ. Sci.: Nano* **2022**, *9*, 767−780.

(4) He, T.; Zhou, Y.; Ding, D.; Rong, S. Engineering Manganese Defects in Mn_3O_4 for Catalytic Oxidation of Carcinogenic Formaldehyde. *ACS Appl. Mater. Interfaces* **2021**, *13*, 29664−29675.

(5) Fan, J.; Niu, X.; Teng, W.; Zhang, P.; Zhang, W.-x.; Zhao, D. Highly Dispersed Fe-Ce Mixed Oxide Catalysts Confined in Mesochannels toward Low-Temperature Oxidation of Formaldehyde. *J. Mater. Chem. A* **2020**, *8*, 17174−17184.

(6) Huang, M.; Li, Y.; Li, M.; Zhao, J.; Zhu, Y.; Wang, C.; Sharma, V. K. Active Site-Directed Tandem Catalysis on Single Platinum Nanoparticles for Efficient and Stable Oxidation of Formaldehyde at Room Temperature. *Environ. Sci. Technol.* **2019**, *53*, 3610−3619.

(7) Chen, J.; Yan, D.; Xu, Z.; Chen, X.; Xu, W.; Jia, H.; Chen, J.; et al. A Novel Redox Precipitation to Synthesize Au-Doped alpha-MnO_2 with High Dispersion toward Low-Temperature Oxidation of Formaldehyde. *Environ. Sci. Technol.* **2018**, *52*, 4728−4737.

(8) Wang, Y.; Liu, K.; Wu, J.; Hu, Z.; Huang, L.; Zhou, J.; Ishihara, T.; Guo, L. Unveiling the Effects of Alkali Metal Ions Intercalated in Layered MnO_2 for Formaldehyde Catalytic Oxidation. *ACS Catal.* **2020**, *10*, 10021−10031.

(9) Wang, Y.; Ye, J.; Jiang, C.; Le, Y.; Cheng, B.; Yu, J. Hierarchical $NiMn_2O_4$/rGO Composite Nanosheets Decorated with Pt for Low-Temperature Formaldehyde Oxidation. *Environ. Sci.: Nano* **2020**, *7*, 198−209.

(10) Zheng, J. Y.; Zhao, W. K.; Wang, X.; Zheng, Z.; Zhang, Y.; Wang, H.; Yan, H.; Song, X.; Han, C. B. Electric-Enhanced Hydrothermal Synthesis of Manganese Dioxide for the Synergistic Catalytic of Indoor Low-Concentration Formaldehyde at Room Temperature. *Chem. Eng. J.* **2020**, *401*, No. 125790.

(11) Li, Y.; Chen, X.; Wang, C.; Zhang, C.; He, H. Sodium Enhances Ir/TiO_2 Activity for Catalytic Oxidation of Formaldehyde at Ambient Temperature. *ACS Catal.* **2018**, *8*, 11377−11385.

(12) de Falco, G.; Barczak, M.; Montagnaro, F.; Bandosz, T. J. A New Generation of Surface Active Carbon Textiles As Reactive Adsorbents of Indoor Formaldehyde. *ACS Appl. Mater. Interfaces* **2018**, *10*, 8066−8076.

(13) Salthammer, T.; Mentese, S.; Marutzky, R. Formaldehyde in the Indoor Environment. *Chem. Rev.* **2010**, *110*, 2536−2572.

(14) Love, A. M.; Thomas, B.; Specht, S. E.; Hanrahan, M. P.; Venegas, J. M.; Burt, S. P.; Grant, J. T.; Cendejas, M. C.; McDermott, W. P.; Rossini, A. J.; Hermans, I. Probing the Transformation of Boron Nitride Catalysts under Oxidative Dehydrogenation Conditions. *J. Am. Chem. Soc.* **2019**, *141*, 182−190.

(15) Dong, J.; Fu, Q.; Li, H.; Xiao, J.; Yang, B.; Zhang, B.; Bai, Y.; Song, T.; Zhang, R.; Gao, L.; Cai, J.; Zhang, H.; Liu, Z.; Bao, X. Reaction-Induced Strong Metal-Support Interactions between Metals and Inert Boron Nitride Nanosheets. *J. Am. Chem. Soc.* **2020**, *142*, 17167−17174.

(16) Ares, P.; Cea, T.; Holwill, M.; Wang, Y. B.; Roldan, R.; Guinea, F.; Andreeva, D. V.; Fumagalli, L.; Novoselov, K. S.; Woods, C. R. Piezoelectricity in Monolayer Hexagonal Boron Nitride. *Adv. Mater.* **2020**, *32*, No. 1905504.

(17) Yadav, V.; Kulshrestha, V. Boron Nitride: a Promising Material for Proton Exchange Membranes for Energy Applications. *Nanoscale* **2019**, *11*, 12755−12773.

(18) Chen, H.; Yang, Z.; Zhang, Z.; Chen, Z.; Chi, M.; Wang, S.; Fu, J.; Dai, S. Construction of a Nanoporous Highly Crystalline Hexagonal Boron Nitride from an Amorphous Precursor for Catalytic Dehydrogenation. *Angew. Chem., Int. Ed.* **2019**, *58*, 10626−10630.

(19) Ding, Y.; Huang, X.; Yi, X.; Qiao, Y.; Sun, X.; Zheng, A.; Su, D. S. A Heterogeneous Metal-Free Catalyst for Hydrogenation: Lewis Acid-Base Pairs Integrated into a Carbon Lattice. *Angew. Chem., Int. Ed.* **2018**, *57*, 13800−13804.

(20) Cuba-Supanta, G.; Guerrero-Sanchez, J.; Rojas-Tapia, J.; Landauro, C. V.; Takeuchi, N. Formaldehyde Trapping by Radical Initiated Reaction on Hydrogenated Boron Nitride. *Appl. Surf. Sci.* **2019**, *484*, 470−478.

(21) Yang, X.; Li, Q.; Li, L.; Lin, J.; Yang, X.; Yu, C.; Liu, Z.; Fang, Y.; Huang, Y.; Tang, C. CuCo Binary Metal Nanoparticles Supported on Boron Nitride Nanofibers as Highly Efficient Catalysts for Hydrogen Generation from Hydrolysis of Ammonia Borane. *J. Power Sources* **2019**, *431*, 135−143.

(22) Lin, J.; Xu, L.; Huang, Y.; Li, J.; Wang, W.; Feng, C.; Liu, Z.; Xu, X.; Zou, J.; Tang, C. Ultrafine Porous Boron Nitride Nanofibers Synthesized via a Freeze-Drying and Pyrolysis Process and Their Adsorption Properties. *RSC Adv.* **2016**, *6*, 1253−1259.

(23) Ezugwu, C. I.; Zhang, S.; Li, S.; Shi, S.; Li, C.; Verpoort, F.; Yu, J.; Liu, S. Efficient Transformative HCHO Capture by Defective NH_2-UiO-66(Zr) at Room Temperature. *Environ. Sci.: Nano* **2019**, *6*, 2931−2936.

(24) Ye, J.; Zhu, X.; Cheng, B.; Yu, J.; Jiang, C. Few-Layered Graphene-like Boron Nitride: A Highly Efficient Adsorbent for Indoor Formaldehyde Removal. *Environ. Sci. Technol. Lett.* **2017**, *4*, 20−25.

(25) Lei, W.; Portehault, D.; Liu, D.; Qin, S.; Chen, Y. Porous Boron Nitride Nanosheets for Effective Water Cleaning. *Nat. Commun.* **2013**, *4*, No. 1777.

(26) Chen, D.; Qu, Z.; Sun, Y.; Gao, K.; Wang, Y. Identification of Reaction Intermediates and Mechanism Responsible for Highly Active HCHO Oxidation on Ag/MCM-41 Catalysts. *Appl. Catal., B* **2013**, *142−143*, 838−848.

(27) Sun, S.; Ding, J.; Bao, J.; Gao, C.; Qi, Z.; Li, C. Photocatalytic Oxidation of Gaseous Formaldehyde on TiO_2: An In Situ DRIFTS Study. *Catal. Lett.* **2010**, *137*, 239−246.

(28) Wang, W.; Xu, D.; Cheng, B.; Yu, J.; Jiang, C. Hybrid Carbon@ TiO_2 Hollow Spheres with Enhanced Photocatalytic CO_2 Reduction Activity. *J. Mater. Chem. A* **2017**, *5*, 5020−5029.

(29) Kattel, S.; Yan, B.; Yang, Y.; Chen, J. G.; Liu, P. Optimizing Binding Energies of Key Intermediates for CO_2 Hydrogenation to Methanol over Oxide-Supported Copper. *J. Am. Chem. Soc.* **2016**, *138*, 12440−12450.

(30) Ma, Y.; Zhang, G. Sepiolite Nanofiber-Supported Platinum Nanoparticle Catalysts toward the Catalytic Oxidation of Formaldehyde at Ambient Temperature: Efficient and Stable Performance and Mechanism. *Chem. Eng. J.* **2016**, *288*, 70−78.